

Multiple superconducting transitions in the $\text{Sr}_3\text{Ru}_2\text{O}_7$ region of $\text{Sr}_3\text{Ru}_2\text{O}_7 - \text{Sr}_2\text{RuO}_4$ eutectic crystals

S. Kittaka,¹ S. Fusanobori,¹ S. Yonezawa,¹ H. Yaguchi,¹ Y. Maeno,^{1,2} R. Fittipaldi,^{1,2,3} and A. Vecchione^{1,2,3}

¹*Department of Physics, Kyoto University, Kyoto 606-8502, Japan*

²*International Innovation Center, Kyoto University, Kyoto 606-8501, Japan*

³*CNR-INFM Regional Laboratory "SuperMat" and Department of Physics University of Salerno, Baronissi (Sa), Italy*

(Dated: October 22, 2021)

We report superconducting properties of $\text{Sr}_3\text{Ru}_2\text{O}_7 - \text{Sr}_2\text{RuO}_4$ eutectic crystals, consisting of the spin-triplet superconductor Sr_2RuO_4 with a monolayer stacking of RuO_2 planes and the metamagnetic normal metal $\text{Sr}_3\text{Ru}_2\text{O}_7$ with a bilayer stacking. Although $\text{Sr}_3\text{Ru}_2\text{O}_7$ has not been reported to exhibit superconductivity so far, our AC susceptibility measurements revealed multiple superconducting transitions occurring in the $\text{Sr}_3\text{Ru}_2\text{O}_7$ region of the eutectic crystals. The diamagnetic shielding essentially reached the full fraction at low AC fields parallel to the c axis. However, both the shielding fraction and the onset temperature are easily suppressed by AC fields of larger than 0.1 mT-rms and no anomaly was observed in the specific heat. Moreover, the critical field curves of these transitions have a positive curvature near zero fields, which is different from the upper critical field curve of the bulk Sr_2RuO_4 . These facts suggest that the superconductivity observed in the $\text{Sr}_3\text{Ru}_2\text{O}_7$ region is not a bulk property. To explain these experimental results, we propose the scenario that stacking RuO_2 planes, the building block of superconducting Sr_2RuO_4 , are contained in the $\text{Sr}_3\text{Ru}_2\text{O}_7$ region as stacking faults.

PACS numbers: 74.70.Pq, 74.50.+r, 74.81.Bd

I. INTRODUCTION

The layered perovskite superconductor Sr_2RuO_4 ($T_c = 1.5$ K), isostructural to the high- T_c cuprate $\text{La}_{2-x}\text{Sr}_x\text{CuO}_4$, is now believed to be a spin-triplet superconductor with broken time-reversal symmetry based on various experimental results.^{1,2,3,4,5} After the discovery of superconductivity in Sr_2RuO_4 , two types of eutectic solidification systems containing Sr_2RuO_4 have been grown: $\text{Sr}_2\text{RuO}_4 - \text{Ru}$ ⁶ and $\text{Sr}_3\text{Ru}_2\text{O}_7 - \text{Sr}_2\text{RuO}_4$ ⁷ These eutectic systems are also interesting because they exhibit unusual superconducting features.

The $\text{Sr}_2\text{RuO}_4 - \text{Ru}$ eutectic system,⁶ in which lamellae of Ru metal are embedded in Sr_2RuO_4 , exhibits a large enhancement of T_c . AC susceptibility measurements⁶ revealed a broad diamagnetic transition with an onset temperature as high as 3 K, which is twice higher than those of best-quality Sr_2RuO_4 single crystals. Therefore, this eutectic is referred to as the 3-K phase. However, specific heat measurements⁸ revealed that the volume fraction of the superconductivity associated with the 3-K phase is very small. Measurements of the tunneling conductance between Sr_2RuO_4 and a single Ru lamella^{9,10} support that the superconductivity with an enhanced T_c occurs in the boundaries between Sr_2RuO_4 and embedded Ru lamellae.

We have recently succeeded in growing another Sr_2RuO_4 -based eutectic system⁷: $\text{Sr}_3\text{Ru}_2\text{O}_7 - \text{Sr}_2\text{RuO}_4$. This eutectic system consists of the spin-triplet superconductor Sr_2RuO_4 with a monolayer stacking of RuO_2 planes and the metamagnetic normal metal^{11,12} $\text{Sr}_3\text{Ru}_2\text{O}_7$, which consists of a bilayer stacking. X-ray diffraction analyses of the $\text{Sr}_3\text{Ru}_2\text{O}_7 - \text{Sr}_2\text{RuO}_4$ eutectic crystals indicated that the directions not only of the c axis but also of the in-plane axes of Sr_2RuO_4 and $\text{Sr}_3\text{Ru}_2\text{O}_7$ are common in the eutectic crystals.⁷ The superconductivity observed in this eutectic crystal also exhibits interesting features. AC susceptibility measurements⁷ of an eutectic sample containing a number of Sr_2RuO_4 and $\text{Sr}_3\text{Ru}_2\text{O}_7$

domains revealed that a superconducting transition occurs at 1.43 K and the diamagnetic shielding fraction keeps increasing upon cooling well below T_c . It was speculated that this additional diamagnetic signal was due to a proximity effect into $\text{Sr}_3\text{Ru}_2\text{O}_7$ from superconducting Sr_2RuO_4 .⁷

Subsequently, a finite superconducting critical current in a $\text{Sr}_3\text{Ru}_2\text{O}_7 - \text{Sr}_2\text{RuO}_4$ eutectic system containing many Sr_2RuO_4 and $\text{Sr}_3\text{Ru}_2\text{O}_7$ domains was observed by Hooper *et al.*¹³ Their finding appears to indicate that $\text{Sr}_3\text{Ru}_2\text{O}_7$ domains are also superconducting. They suggested the possibility of a proximity effect in the $\text{Sr}_3\text{Ru}_2\text{O}_7$ regions with an unusually-long coherence length. In fact, the coherence length ξ_N in $\text{Sr}_3\text{Ru}_2\text{O}_7$ due to a proximity effect must be as long as the size of $\text{Sr}_3\text{Ru}_2\text{O}_7$ domains, a few hundred micro meters, if supercurrent flows across the $\text{Sr}_3\text{Ru}_2\text{O}_7$ regions. However, the conventional coherence length of a proximity effect in a clean limit approximation yields $\xi_N \sim 0.17 \mu\text{m}$ at 0.3 K. This value of the conventional coherence length is too short to account for the superconductivity in $\text{Sr}_3\text{Ru}_2\text{O}_7$.

In the present study, we investigated the temperature dependence of AC susceptibility at various AC and DC fields, using $\text{Sr}_3\text{Ru}_2\text{O}_7 - \text{Sr}_2\text{RuO}_4$ eutectic samples consisting of one Sr_2RuO_4 region and one $\text{Sr}_3\text{Ru}_2\text{O}_7$ region with a single boundary between them (e. g. see the insets of Fig. 1(a) and Fig. 2). Measurements of these samples revealed that the apparent superconducting volume fraction of the $\text{Sr}_3\text{Ru}_2\text{O}_7 - \text{Sr}_2\text{RuO}_4$ eutectic sample was as large as 100%. In order to test the proximity scenario, we performed similar measurements with the $\text{Sr}_3\text{Ru}_2\text{O}_7$ region cut from a eutectic crystal and, surprisingly, we also observed superconductivity with a very large apparent volume fraction. These results indicate that the superconductivity with a large apparent volume fraction occurs in the $\text{Sr}_3\text{Ru}_2\text{O}_7$ region and that its origin cannot be attributed to a proximity effect from the bulk Sr_2RuO_4 region. In addition, we did not observe any anomaly in the specific heat of the $\text{Sr}_3\text{Ru}_2\text{O}_7$ region. Also, we calculated the

temperature dependence of the AC susceptibility based on a multiple superconductor model (Scenario II in Sec. IV) and obtained calculated results which well match our experimental results.

II. EXPERIMENTAL

In this paper, we mainly present data which were obtained using a sample cut from a $\text{Sr}_3\text{Ru}_2\text{O}_7$ – Sr_2RuO_4 eutectic crystal (batch No. Cfv07 in Ref. 7), grown with a floating-zone furnace. We carefully chose a $\text{Sr}_3\text{Ru}_2\text{O}_7$ – Sr_2RuO_4 eutectic part which has only one boundary between Sr_2RuO_4 and $\text{Sr}_3\text{Ru}_2\text{O}_7$ (hereafter referred to as Sample 1). The size of Sample 1 was approximately $1.5 \times 0.7 \times 0.3 \text{ mm}^3$. The inset of Fig. 1(a) shows polarized light optical microscopy (PLOM) images of polished ab planes of Sample 1. The darker area of the sample is the Sr_2RuO_4 region and the brighter area is the $\text{Sr}_3\text{Ru}_2\text{O}_7$ region, which was confirmed by a high resolution X-ray diffractometer⁷ and energy dispersive X-ray (EDX) analysis. Sample 1 certainly consists of one bulk Sr_2RuO_4 region and one bulk $\text{Sr}_3\text{Ru}_2\text{O}_7$ region because the top and bottom surfaces have the same eutectic pattern. In order to check the reproducibility of experimental results, we performed measurements with more than ten eutectic samples (one of them is Sample 2 from the batch Cfv07, shown in the inset of Fig. 2(c)). Eutectic samples from different batches exhibit qualitatively the same behavior, too.

We measured AC magnetic susceptibility $\chi_{AC} = \chi' + i\chi''$ by a mutual-inductance technique using a lock-in amplifier at various frequencies ranging from 19 Hz to 3011 Hz. The data shown below were all taken at 3011 Hz because the frequency dependence of χ_{AC} was found to be insignificant. The AC susceptibility was measured down to 0.3 K using a ^3He cryostat with a 2-T magnet (Oxford Instruments), and down to 20 mK using a ^3He - ^4He dilution refrigerator (Cryoconcept) with an 11-T magnet (Oxford Instruments). The AC field H_{AC} was applied parallel to the c axis or the ab plane with a small coil (40 μT / mA), and the DC field H_{DC} was applied parallel to H_{AC} . In this paper, we mainly report results under magnetic fields parallel to the c axis. When we measured χ_{AC} in zero DC field, we used a high-permeability-metal shield to exclude the geomagnetic field of about 50 μT . The resultant residual field in this shield was estimated to be lower than 0.1 μT .

We also measured specific heat c_p of eutectic samples by a thermal relaxation method with a commercial calorimeter (Quantum Design, PPMS) from 30 K to 0.8 K. The $\text{Sr}_3\text{Ru}_2\text{O}_7$ – Sr_2RuO_4 eutectic crystals were characterized by X-ray diffraction (XRD) with $\text{CuK}_{\alpha 1}$ radiation and EDX analysis.

III. RESULTS

AC susceptibility measurement

Figure 1(a) shows the temperature dependence of the AC susceptibility of Sample 1 ($\text{Sr}_3\text{Ru}_2\text{O}_7$ – Sr_2RuO_4 eutectic

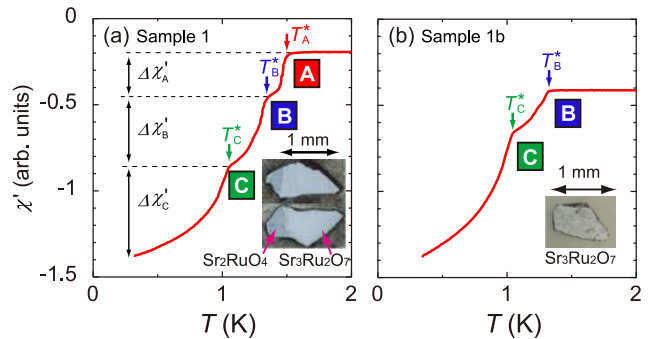


FIG. 1: (Color online) Temperature dependence of the real part of the AC susceptibility at $\mu_0 H_{AC} = 0.58 \mu\text{T-rms}$ and $\mu_0 H_{DC} = 0 \text{ T}$: (a) for Sample 1 ($\text{Sr}_3\text{Ru}_2\text{O}_7$ – Sr_2RuO_4 eutectic); (b) for Sample 1b (i. e. the $\text{Sr}_3\text{Ru}_2\text{O}_7$ region cut from Sample 1). Insets are PLOM images of the samples.

crystal) under $\mu_0 H_{AC} = 0.58 \mu\text{T-rms}$ and $\mu_0 H_{DC} = 0 \text{ T}$ with a high-permeability metal shield. In this measurement, we observed three steep changes of the diamagnetic signal in χ' , which hereafter we call transitions A, B, and C. The transition temperatures, defined as the onset temperatures of the transitions in χ' , were 1.48 K, 1.33 K, and 1.04 K, and are hereafter labeled T_A^* , T_B^* , and T_C^* , respectively. Although more peaks were observed in χ'' (marked with the arrows in Fig. 2(b)), we mainly focus on the transitions A, B, and C. It was difficult to evaluate the shielding fraction accurately because of the large demagnetization factor of the sample. By comparing the diamagnetic signal $\Delta\chi'$ of Sample 1, which is equal to $\Delta\chi'_A + \Delta\chi'_B + \Delta\chi'_C$ as shown in Fig. 1(a), with that of a pure Sr_2RuO_4 crystal with dimensions similar to that of Sample 1, we evaluated the apparent shielding fraction of Sample 1 to be approximately 100% at 0.3 K. This large shielding fraction implies that the superconducting screening current flows not only in the Sr_2RuO_4 part of the sample but also in most of the $\text{Sr}_3\text{Ru}_2\text{O}_7$ region.

In order to clarify whether or not this superconductivity is attributed to an unusual proximity effect from the boundary of the bulk Sr_2RuO_4 , we completely removed the bulk Sr_2RuO_4 part from Sample 1, hereafter labeled Sample 1b. The dimension of Sample 1b is approximately $1.0 \times 0.6 \times 0.15 \text{ mm}^3$. The inset of Fig. 1(b) is a PLOM image of Sample 1b. As presented in Fig. 1(b), two of the superconducting transitions were still observed in Sample 1b. The transition temperatures were 1.32 K and 1.04 K, well corresponding to T_B^* and T_C^* in Sample 1. The absence of transition A in Sample 1b proves that transition A originates from the bulk Sr_2RuO_4 part of Sample 1 and that the transitions B and C occur in the $\text{Sr}_3\text{Ru}_2\text{O}_7$ region. The apparent shielding fraction of Sample 1b was estimated to be 90% for $H \parallel c$ from the diamagnetic signal $\Delta\chi' (= \Delta\chi'_B + \Delta\chi'_C)$. In contrast, it was estimated to be less than 1% for $H \parallel ab$ (not shown). These facts indicate that the superconducting screening current mainly flows within the ab planes. From these measurements, we conclude that the $\text{Sr}_3\text{Ru}_2\text{O}_7$ region in the eutectic crystal has multiple superconducting transitions though pure $\text{Sr}_3\text{Ru}_2\text{O}_7$ has

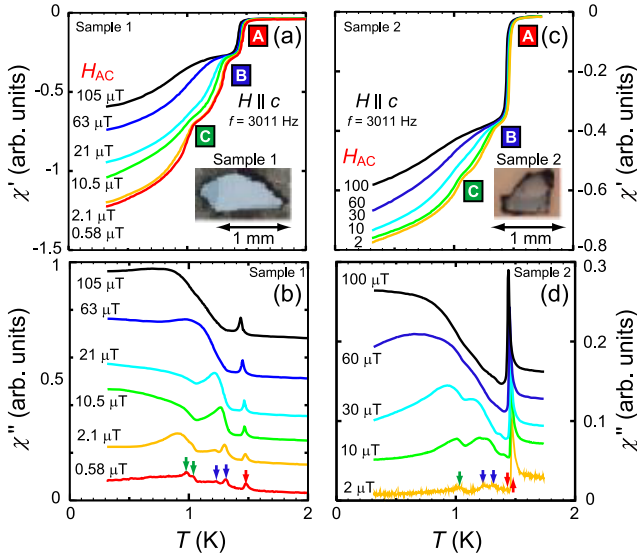


FIG. 2: (Color online) Temperature dependence of the AC susceptibility of $\text{Sr}_3\text{Ru}_2\text{O}_7 - \text{Sr}_2\text{RuO}_4$ eutectic crystals in various AC magnetic fields ($H_{AC} \parallel c$, $\mu_0 H_{DC} = 0$ T). Figures (a) and (b) represent the real and imaginary parts of χ_{AC} of Sample 1, respectively. Figures (c) and (d) represent those of Sample 2. Insets are PLOM images of the samples. The numbers labeling the curves give the applied AC field amplitude $\mu_0 H_{AC}$ in $\mu\text{T-rms}$.

not been reported to become superconducting down to 20 mK (Ref. 11). Moreover, it is clear that the origin of the superconductivity observed in the $\text{Sr}_3\text{Ru}_2\text{O}_7$ region is not a proximity effect from the bulk Sr_2RuO_4 part of eutectic crystals across the boundary.

We revealed that *both* T^* and $\Delta\chi'$ of the transitions B and C are extremely sensitive to the amplitude of H_{AC} when H_{AC} is parallel to the c axis. Figures 2(a) and (b) represent χ' and χ'' of Sample 1 in different AC magnetic fields. We normalized the obtained signals with respect to the strength of H_{AC} . As shown in Fig. 2(a), T_A^* and $\Delta\chi'_A$ hardly depends on H_{AC} up to 100 $\mu\text{T-rms}$. In contrast, $\Delta\chi'_B$ and $\Delta\chi'_C$ are severely suppressed by H_{AC} of less than 100 $\mu\text{T-rms}$. In addition, T_B^* and T_C^* are easily shifted toward lower temperatures with increasing AC field amplitude. As represented in Figs. 2(c) and (d), we reproducibly observed these features in other samples. However, when H_{AC} is applied parallel to the ab plane, T^* and $\Delta\chi'$ of the transitions B and C are not sensitive to H_{AC} of less than 100 $\mu\text{T-rms}$.

In order to obtain more information on the transitions B and C, we measured the DC field dependence of χ_{AC} for Sample 1b. Figure 3 shows the temperature dependence of χ' and χ'' at various DC fields and Fig. 4 presents the DC field dependence of χ' at several temperatures for Sample 1b. In these measurements, we fixed the amplitude of H_{AC} to 1 $\mu\text{T-rms}$, and both H_{AC} and H_{DC} were applied parallel to the c axis. These measurements revealed that T_B^* and T_C^* are *not* severely suppressed, but $\Delta\chi'_B$ and $\Delta\chi'_C$ are easily suppressed by H_{DC} .

We obtained the $H-T$ phase diagram for $H \parallel c$, which is plotted in Fig. 5. Here, the critical fields of the transitions B and C are labeled H_B^* and H_C^* , respectively, which are defined

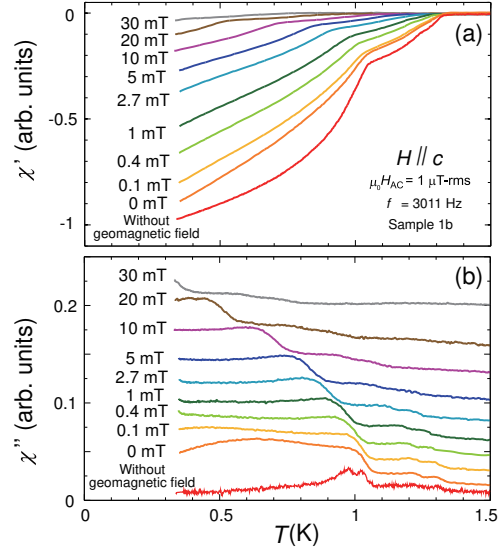


FIG. 3: (Color online) Temperature dependence of the (a) real and (b) imaginary parts of χ_{AC} of Sample 1b in different DC fields.

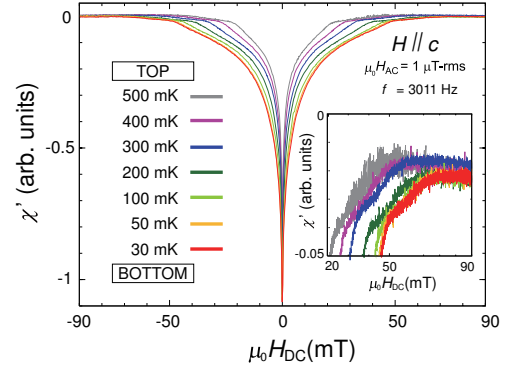


FIG. 4: (Color online) The DC field dependence of the real part of χ_{AC} of Sample 1b. The inset gives an enlarged view near onset. In order to take into account the residual fields in our equipment, which is estimated to be approximately 1 mT, we determined zero field as a field at which χ' becomes minimum.

as the onset of χ' . For comparison, we included the upper critical field H_{c2} of bulk Sr_2RuO_4 determined by specific heat measurements¹⁴ and those determined by AC susceptibility measurements¹⁵ in this figure. The extrapolation of $\mu_0 H_B^*$ to $T = 0$ yields 75 mT, which is nearly equal to $\mu_0 H_{c2}(T = 0)$ of bulk Sr_2RuO_4 .

However, temperature dependences of H_B^* and of H_C^* are qualitatively different from $H_{c2}(T)$ of bulk Sr_2RuO_4 . Fitting the function $H_{c2}(T) = \alpha(1 - T/T_c)^n$ to the H_{c2} data from specific heat measurements of bulk Sr_2RuO_4 yields $n = 1.0$ for $H \parallel c$ near $H_{DC} = 0$, where α and n are adjustable parameters. In contrast, both H_B^* and H_C^* exhibit temperature dependences with positive curvatures ($n = 1.6$ for H_B^* , $n = 1.5$ for H_C^*) near $H_{DC} = 0$ and then increase approximately linearly with decreasing temperature. Such behavior suggests that the transitions B and C are of a similar origin, but different from the

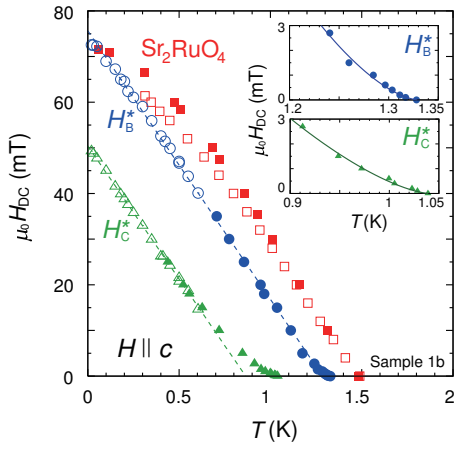


FIG. 5: (Color online) H - T phase diagram of Sample 1b for $H_{AC} \parallel H_{DC} \parallel c$ determined from the AC susceptibility measurements. The circles and triangles represent the critical fields of the transitions B and C, respectively. The open symbols are obtained from field sweep data and the closed symbols from temperature sweep data. H_{c2} of bulk Sr_2RuO_4 from specific-heat data (Ref. 14, closed squares) and from AC susceptibility measurements (Ref. 15, open squares) are also plotted. The insets show the low-field region below 3 mT. The solid lines represent fits of the data close to $T_0^* \equiv T^*(H_{DC} = 0)$ using the function $\alpha(1 - T/T_0^*)^n$. The dashed lines present results of linear fittings to the data between 0 K and $0.7 T_0^*$.

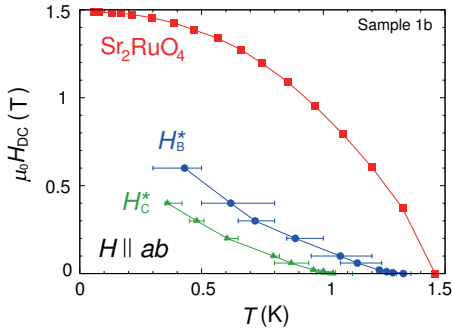


FIG. 6: (Color online) H - T phase diagram of Sample 1b for $H_{AC} \parallel H_{DC} \parallel ab$. The circle and triangular symbols represent the critical fields of the transitions B and C determined by the AC susceptibility measurements, respectively. The upper critical fields H_{c2} of bulk Sr_2RuO_4 are obtained from AC susceptibility measurements (Ref. 15, squares). The solid lines are guides to the eye.

bulk superconducting transition.

We also constructed the H - T phase diagram for $H \parallel ab$, as shown in Fig. 6. In this measurement, both H_{AC} of 20 μT -rms and H_{DC} were applied parallel to the ab plane. Both the temperature dependence of H_B^* and of H_C^* exhibit a positive curvature near $H_{DC} = 0$, similar to those for $H \parallel c$. The critical field anisotropies $H_{\parallel ab}^*/H_{\parallel c}^*$ of the transitions B and C are approximately 13 at 0.3 K, which is somewhat smaller than that observed for bulk Sr_2RuO_4 (Ref. 16: $H_{c2\parallel ab}/H_{c2\parallel c} \sim 20$).

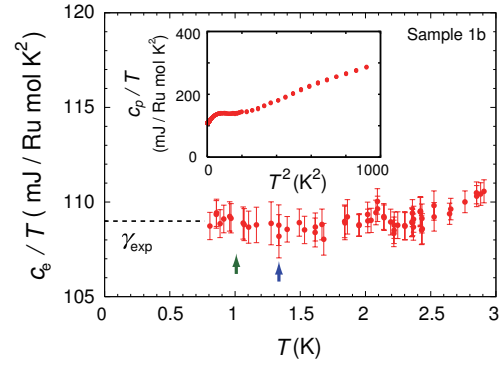


FIG. 7: (Color online) Temperature dependence of the electronic specific heat divided by temperature c_e/T of Sample 1b. The inset represents c_p/T plotted against T^2 . The arrows mark T_B^* and T_C^* of this sample at zero field.

Specific heat measurement

We measured the specific heat of Sample 1b (with a mass $m = 0.472$ mg), which exhibits nearly full diamagnetic shielding in our AC susceptibility measurements for $H \parallel c$. This specific heat measurement was performed in zero field, but the geomagnetic field and the residual field of the magnet (≤ 1 mT) were not shielded. The main panel of Fig. 7 shows the electronic specific heat divided by temperature for Sample 1b. There is no anomaly at T_B^* and T_C^* . Therefore, we conclude that the actual volume fraction of the superconductivity observed in the apparent $\text{Sr}_3\text{Ru}_2\text{O}_7$ region is very small.

In order to obtain the electronic specific-heat coefficient γ_{exp} of Sample 1b and check the molar ratio x of Sr_2RuO_4 contained in Sample 1b, we used an effective weight per Ru-mol M_{eff} , which is defined as $M_{\text{eff}}(x) = xM_{214} + (1-x)M_{327}/2$, where M_{214} and M_{327} are the molar weights of a formula unit of Sr_2RuO_4 and $\text{Sr}_3\text{Ru}_2\text{O}_7$, respectively. We determined γ_{exp} , which is obtained from the relation $\gamma_{\text{exp}}(x) = (C_p/T)m/M_{\text{eff}}(x)$ (C_p is the heat capacity of the sample), self-consistently by adjusting x so that $\gamma_{\text{exp}}(x)$ becomes equal to $x\gamma_{214} + (1-x)\gamma_{327}$. Here, γ_{214} and γ_{327} represents the electronic specific-heat coefficient of bulk Sr_2RuO_4 ($\gamma_{214} = 38$ mJ/Ru-mol K^2 (Ref. 17)) and $\text{Sr}_3\text{Ru}_2\text{O}_7$ ($\gamma_{327} = 110$ mJ/Ru-mol K^2 (Ref. 18)), respectively. As a result, we obtained $\gamma_{\text{exp}} \sim 109$ mJ/Ru-mol K^2 and $x = 0.016 \pm 0.008$. In addition, the overall temperature dependence of the total specific heat c_p of Sample 1b presented in the inset of Fig. 7 is consistent with previous reports¹⁸ for pure $\text{Sr}_3\text{Ru}_2\text{O}_7$. These facts imply that the $\text{Sr}_3\text{Ru}_2\text{O}_7$ region of the eutectic crystals is almost the same as pure $\text{Sr}_3\text{Ru}_2\text{O}_7$.

PLOM, EDX, and XRD analyses

In order to characterize the sample in more details, we took PLOM images, and performed elemental composition analysis with an EDX spectrometer and XRD analysis. From PLOM images and elemental composition analysis, we did

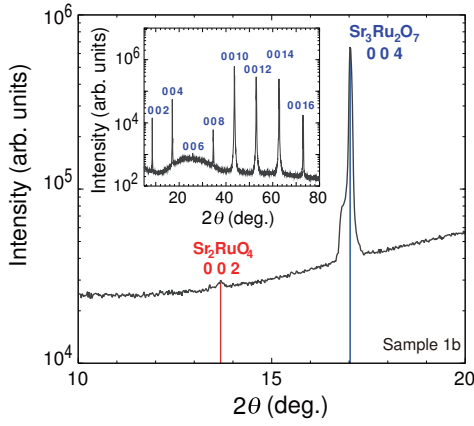


FIG. 8: (Color online) X-ray diffraction pattern for the ab plane of Sample 1b. Note that the vertical axis is in a logarithmic scale.

not find Sr_2RuO_4 and the whole sample seemed to consist of $\text{Sr}_3\text{Ru}_2\text{O}_7$. We note that we cannot rule out the presence of Sr_2RuO_4 parts with a size of less than about $1 \mu\text{m}$, which is the experimental resolution limit of our instruments. In the XRD pattern for the ab plane of Sample 1b, as shown in Fig. 8, a very weak $\langle 002 \rangle$ peak of Sr_2RuO_4 was detected in addition to strong $\text{Sr}_3\text{Ru}_2\text{O}_7$ peaks. The observed peak intensity suggests that less than a few percent Sr_2RuO_4 is contained at least in the surface region of Sample 1b. This possible small content of Sr_2RuO_4 is consistent with the results of the specific heat measurement.

IV. DISCUSSION

In order to discuss why superconductivity is observed in the $\text{Sr}_3\text{Ru}_2\text{O}_7$ region of eutectic crystals, we assumed two scenarios (Scenario I and II) and calculated $\chi_{AC}(T)$ for $H \parallel c$ using simplified models.

Scenario I

First, we note that our results of $\chi_{AC}(T)$ is somewhat similar to those of granular superconductors, in which Josephson-type weak links are formed among superconducting grains. For example, polycrystals of $\text{Tl}_2\text{Ba}_2\text{Ca}_2\text{Cu}_3\text{O}_y$, prepared by a suitable sintering process, consist of agglomerates of grains whose typical size is approximately $5 \mu\text{m}$.¹⁹ These grains are arranged randomly and connected strongly by nonstoichiometric interfacial materials. When such polycrystals are cooled below T_c of the grains, the grains first become superconducting. Upon further cooling, Josephson-type weak links are formed among the grains. Therefore, shielding currents flow in inter-grain paths and magnetic flux is excluded from the inter-grain regions. As a result, two transitions, which are attributed to intra-grain and inter-grain superconductivity, are observed in $\chi_{AC}(T)$ and the transition temperature of inter-grain superconductivity is sensitive to H_{AC} than to H_{DC} .¹⁹

These features are observed in our results. Therefore, we first discuss the scenario that small superconducting Sr_2RuO_4 grains are embedded in the $\text{Sr}_3\text{Ru}_2\text{O}_7$ region of the eutectic crystals and superconducting networks are formed among them along ab planes (Fig. 9 left; Scenario I).

Here, let us introduce a model developed by Müller and Yang *et al.* in order to calculate χ_{AC} of granular superconductors. Yang *et al.*¹⁹ calculated $\chi_{AC}(T)$ of polycrystal $\text{Tl}_2\text{Ba}_2\text{Ca}_2\text{Cu}_3\text{O}_y$ by a method similar to Müller's theoretical work,²⁰ and their results well reproduced the experimental findings. Below, we calculate χ' and χ'' in the same way as Yang *et al.*¹⁹ The sample shape is assumed to be a thin slab of thickness $2d$ in the x direction. The length in the y direction and height in the z direction of the sample are assumed to be infinity. The applied field $H_a(t) = \sqrt{2}H_{AC} \cos(\omega t) + H_{DC}$ is parallel to the slab's z direction. To avoid the complication of demagnetization factors, the grains are approximated as infinitely-long superconducting cylinders aligned along the z direction. Instead, effects of finite demagnetization factors are embedded in other parameters as we will explain below. The grain radius is assumed to be the same value $R_g (\ll 2d)$, which represents the average grain radius in the experiments, for the all grains.

The real and imaginary parts of χ_{AC} are expressed as

$$\chi' = \frac{\omega}{\sqrt{2}\pi\mu_0 H_{AC}} \int_0^{2\pi/\omega} \langle B(t) \rangle \cos(\omega t) dt - 1, \quad (1)$$

$$\chi'' = \frac{\omega}{\sqrt{2}\pi\mu_0 H_{AC}} \int_0^{2\pi/\omega} \langle B(t) \rangle \sin(\omega t) dt. \quad (2)$$

Here, $\langle B(t) \rangle$ is the spatial average local flux density over the sample cross-section, and is given by $\langle B(t) \rangle = \langle B_J(t) \rangle_x + \langle\langle B_g(t) \rangle\rangle_{r,x}$. $\langle B_J(t) \rangle_x$ and $\langle\langle B_g(t) \rangle\rangle_{r,x}$ are the spatial average over the sample of the inter-grain flux density $B_J(x, t)$ and that of the average intra-grain flux density threading a cylindrical grain $\langle B_g(x, t) \rangle_r$, respectively. These notations are the same as those given by Müller.²⁰

Let us now derive the inter- and intra-grain magnetic field distribution using the critical state equations²⁰ in order to obtain $\langle B_J(t) \rangle_x$ and $\langle\langle B_g(t) \rangle\rangle_{r,x}$. For the inter-grain regions, magnetic flux density B_J is larger than $\mu_0 H_J$ because magnetic flux is compressed into the inter-grain regions due to the diamagnetism of the superconducting grains. By embedding this effect into the effective permeability μ_{eff} , B_J can be expressed as $B_J = \mu_{\text{eff}}\mu_0 H_J$. The effective permeability $\mu_{\text{eff}}(T)$ is written as^{21,22,23} $\mu_{\text{eff}}(T) = f_n + f_s F(R_g/\lambda_g(T))$, where $\lambda_g(T)$ denotes the London penetration depth of the superconducting grains, which depends on T as $\lambda_g(T) = \lambda_g(0)[1 - (T/T_{cg})^4]^{-1/2}$. The factor f_s is the area fraction of the projection of grains onto a plane normal to the magnetic field, and f_n is that of inter-grain regions ($f_n = 1 - f_s$). The flux penetration within the surface penetration depth of the grains in the Meissner state is taken into account via $F(x)$, which is written as $F(x) = 2I_1(x)/(xI_0(x))$; I_0 and I_1 are the modified Bessel functions of the first kind. The inter-grain magnetic field distribution H_J is given by the solution of the critical state equations²⁰

$$J_{cJ}(x, t) = \frac{\alpha_J(T)}{\mu_{\text{eff}}(T)\mu_0} \frac{1}{|H_J(x, t)| + H_{0J}}, \quad (3)$$

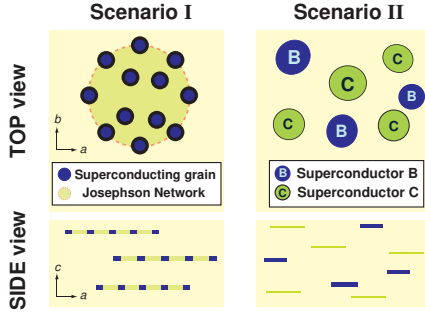


FIG. 9: (Color online) Scenarios for the superconductivity observed in the $\text{Sr}_3\text{Ru}_2\text{O}_7$ region of eutectic crystals are depicted. The superconducting regions are probably distributed along the ab planes because the shielding currents mainly flow within the ab planes. Such a layered arrangement is not taken into account in our simple model calculations.

$$\frac{dH_J(x, t)}{dx} = \pm J_{cJ}(x, t), \quad (4)$$

where we assume that the pinning force α_J of a vortex is equal to the Lorentz force.²⁴ The pinning force α_J is assumed to depend on T as¹⁹ $\alpha_J(T)/\mu_{\text{eff}}(T) = \alpha_J(0)(1 - T/T_{cJ})^2/\mu_{\text{eff}}(0)$, and H_{0J} is a positive parameter. The \pm signs account for the outward or inward motion of vortices with decreasing or increasing applied magnetic field, respectively.

While for the intra-grain regions, we also assume the critical state. Here, we used $B_g(r, x, t)$, which is equal to $\mu_0(H_g^{\text{ext}}(x, t) + M_g(r, x, t))$, where H_g^{ext} is the magnetic field at the boundary of a grain and M_g is the local magnetization in the grain, because M_g is finite in the grains. $B_g(r, x, t)$, which is equivalent to $\mu_0 H_g(r, x, t)$ in Müller's work,²⁰ is obtained by the solution of the equations

$$J_{cg}(r, x, t) = \frac{\alpha_g(T)}{|B_g(r, x, t)| + B_{0g}}, \quad (5)$$

$$\frac{1}{\mu_0} \frac{dB_g(r, x, t)}{dr} = \pm J_{cg}(r, x, t). \quad (6)$$

In this case, the pinning force α_g is assumed²⁰ to be $\alpha_g(T) = \alpha_g(0)[1 - (T/T_{cg})^2]^2$. B_{0g} is a positive parameter. We note that the effects of demagnetization factors are embedded in $\alpha_g(0)$ and B_{0g} . For example, if the demagnetization factor is large, $\alpha_g(0)/B_{0g}$ would become large. Solving Eqs. (3)–(6), we obtain $H_J(x, t)$ and $B_g(r, x, t)$, from which we can calculate $\langle B_J(t) \rangle_x$ and $\langle\langle B_g(t) \rangle\rangle_{r,x}$, as shown in Ref. 20. By putting these quantities into Eqs. (1) and (2), we obtain χ' and χ'' . Hereafter, we call this model the Müller-Yang model.

In this calculation, we fixed T_{cg} , T_{cJ} , and d to the values obtained from the present measurements, i. e. $T_{cg} = 1.34$ K, $T_{cJ} = 1.10$ K, and $d = 1$ mm, and $\lambda_g(0)$ to the known value for the bulk Sr_2RuO_4 . We varied the other parameters so that the calculated results best agree with our experiments: f_n and R_g are changed manually so that we reproduce the behavior observed in weak magnetic fields at temperatures around T_{cg} , H_{0J} and α_{0J} are adjusted so that we reproduce the AC magnetic field dependence of the step in χ' and the peak in χ'' at

transition C, and B_{0g} and α_{0g} are adjusted so that we reproduce the AC magnetic field dependence of transition B.

The calculated results based on the Müller-Yang model are shown in Figs. 10(c) and (d). In our calculations, R_g was estimated to be $2 \mu\text{m}$, and f_n was estimated to be 60%. These parameters are similar to those used in Müller's work.²⁰ However, our calculation contains several inconsistencies with the experiments. First, the behavior of transition C is different from that of the Josephson weak-link network, as shown in Figs. 10(a)–(d). In our calculations, T_C^* is shifted toward lower temperatures, but $\Delta\chi'_C$ is not severely suppressed with increasing the amplitude of H_{AC} , which is typical weak-link behavior. In contrast, in our experiments, both T_C^* and $\Delta\chi'_C$ are easily suppressed with increasing the strength of H_{AC} . Moreover, as shown in Figs. 5 and 6, the temperature dependences of H_B^* and of H_C^* are qualitatively similar, and are different from $H_{c2}(T)$ of bulk Sr_2RuO_4 . This behavior is not consistent with a model of granular superconductivity, in which T_c of grains and T_c of inter-grain region should exhibit totally-different field dependences. These results suggest that the Josephson-network scenario does not seem to be suitable for the superconductivity in the $\text{Sr}_3\text{Ru}_2\text{O}_7$ region of the eutectic crystals.

Scenario II

The second scenario assumes that no superconducting network is formed, but superconductors of thin-film shapes with multiple T_c 's are contained in the $\text{Sr}_3\text{Ru}_2\text{O}_7$ region. We consider that stacked monolayers of RuO_2 planes, the building block of superconducting Sr_2RuO_4 , are contained in the $\text{Sr}_3\text{Ru}_2\text{O}_7$ region as stacking faults, and exhibit superconductivity with different T_c 's depending on the number of monolayers contained in a stacking unit. Although fabrications of superconducting thin films of Sr_2RuO_4 have not been reported so far, it was reported that T_c of thin $\text{YBa}_2\text{Cu}_3\text{O}_{7-x}$ films depends on their thickness.²⁵ It is also known that the $H_{c2}(T)$ curve of quasi-two-dimensional superconductors for $H_{DC} \perp$ layer,²⁶ which can be regarded as a stacking of thin films, has a positive curvature near $H_{DC} = 0$. The thickness of monolayers should be comparable to or less than the coherence length of Sr_2RuO_4 along the c axis (~ 3.3 nm) because the transitions B and C would behave as bulk superconductivity if the thickness were much larger than the coherence length. This scenario is consistent with the fact that we cannot find Sr_2RuO_4 in the $\text{Sr}_3\text{Ru}_2\text{O}_7$ region by EDX analysis and PLOM images because Sr_2RuO_4 slabs with a thickness of several nano meters are too thin to find for our instruments.

Although this scenario appears to be different from the situation of Scenario I, we can still calculate $\chi_{AC}(T)$ using the Müller-Yang model after a slight modification. The modified model, which we call as a multiple superconductor model, assumes that the sample is divided into areas with different T_c 's and $\chi_{AC}(T)$ is calculated in each area using Eqs. (1)–(6) with $\alpha_J(0) = 0$ TAm⁻² and $f_n = 0$. These conditions assume that no superconducting network is formed in the sample. In this model calculation, we considered the AC susceptibility of the sample as $\chi_{AC} = \sum_i p_i \chi_i$, where p_i is the percentage of the i -th

TABLE I: Parameters used in our calculations based on Scenario II. The open squares (\square) mark the parameters that we adjusted to obtain the best fit to our experiments. The closed squares (\blacksquare) label the parameters we fixed in our calculations. “SC1” denotes the superconducting area responsible to the transition B and “SC2” and “SC3” denote those to the transition C.

		SC1	SC2	SC3	
T_{cg}	(K)	1.34	1.10	1.10	\blacksquare
B_{0g}	(μ T)	10	30	200	\square
$\alpha_g(0)$	($\text{T}\text{A}\text{m}^{-2}$)	30000	8000	3000	\square
R_g	(μm)	1	1	1	\square
$\lambda_g(0)$	(μm)	0.18	0.18	0.18	\blacksquare
p_i		0.25	0.35	0.4	\blacksquare

area ($\sum_i p_i = 1$), and χ_i represents the AC susceptibility of the i -th area. It might be more plausible in reality that the thickness of a single Sr_2RuO_4 thin slab is not homogeneous. This possible inhomogeneity was neglected in our calculations.

For Sample 1b, we assumed three kinds of superconductors SC1, SC2, and SC3, with two distinct transition temperatures to reproduce the experiments well. The necessity of introducing SC3 implies that there are two kinds of regions with essentially the same T_c , but with much different J_c values. These different J_c values would be caused by the effects of finite demagnetization factor of thin film because we embedded it into the parameters B_{0g} and $\alpha_g(0)$. However, we consider that the existence of SC3 is not essential because SC3 was not necessary in the calculations for other samples.

In our calculation, the parameters T_{cg} , $\lambda_g(0)$, and p_i were fixed. The other parameters B_{0g} , α_g , and R_g were adjusted manually so that the calculated results best agree with our experiments. The results are summarized in Table I and Figs. 10(e) and (f). Our calculation reproduces the essential features of the experimental findings. For example, the observation that *both* T_c^* and $\Delta\chi'_C$ decrease with increasing the amplitude of H_{AC} is reproduced. Although the critical current density $J_c(0)$ of the pure Sr_2RuO_4 is approximately $500 \text{ A}/\text{cm}^2$ (Ref. 27), that of SC1 was estimated to be $3 \times 10^5 \text{ A}/\text{cm}^2$ from B_{0g} and $\alpha_g(0)$ using Eq. (5). If the thickness of the superconductor also decreases and the critical current density should become large as often observed in thin films. Therefore, such a large $J_c(0)$ may also support the scenario that Sr_2RuO_4 is contained as a thin slab.

No single plane of a monolayer RuO_2 probably covers the whole ab plane. However, the magnetic flux would be excluded from the whole sample for $H \parallel c$ if there are many such layers in the sample. In addition, this scenario does not contradict with our results that the apparent shielding fraction is less than 1% for $H \parallel ab$.

From the discussions above, we consider that this scenario is the most probable one to explain the superconductivity observed in the $\text{Sr}_3\text{Ru}_2\text{O}_7$ region of eutectic crystals. In addition, recently such stacked monolayers of RuO_2 planes have indeed been observed using a transmission electron microscope.²⁸

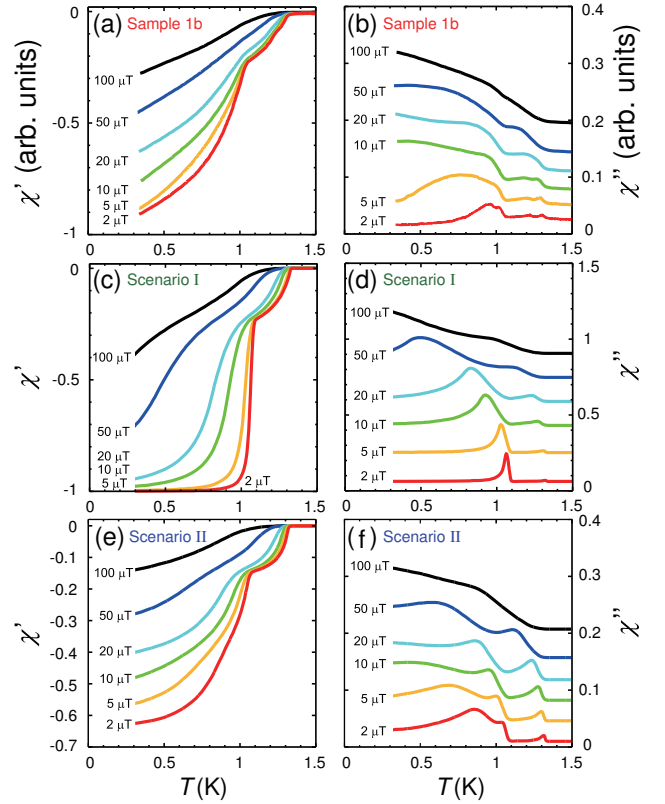


FIG. 10: (Color online) (a), (b) Experimental and (c)-(f) calculated results of $\chi_{AC}(T)$ at various AC magnetic fields in $\mu_0 H_{DC} = 0 \text{ T}$. The numbers labeling the curves indicate the applied AC field amplitude $\mu_0 H_{AC}$ in $\mu\text{T-rms}$.

The possibility of superconducting $\text{Sr}_3\text{Ru}_2\text{O}_7$

Finally, we discuss the possibility that small $\text{Sr}_3\text{Ru}_2\text{O}_7$ parts in the Sample 1b become superconducting, due to a specific arrangement of the RuO_6 octahedra, different from the arrangement realized in bulk $\text{Sr}_3\text{Ru}_2\text{O}_7$. The structure of bulk $\text{Sr}_3\text{Ru}_2\text{O}_7$ contains orthorhombic deformations due to the rotation of the RuO_6 octahedra.^{29,30,31} In Ruddlesden-Popper type ruthenates $\text{Sr}_{n+1}\text{Ru}_n\text{O}_{3n+1}$, it is known that their rotation, tilting, and flattening of RuO_6 octahedra affect the electronic states significantly.^{32,33,34} In fact, the electronic and thermodynamic properties of $\text{Ca}_{2-x}\text{Sr}_x\text{RuO}_4$ are greatly affected by the rotation with varying x (Refs. 34, 35). Degrees of freedom such as the rotation angle or an ordering pattern of rotations might be left in $\text{Sr}_3\text{Ru}_2\text{O}_7$ under certain circumstances. Indeed, different ordering patterns of rotations have been reported in powder samples.^{29,30,31} Therefore, it is possible that some small parts of $\text{Sr}_3\text{Ru}_2\text{O}_7$ with a certain arrangement of RuO_6 octahedra are superconducting and that these parts play roles of superconductors in Scenario II. However, we did not obtain any direct structural evidence to conclude that octahedral rotation and/or tilting in eutectic $\text{Sr}_3\text{Ru}_2\text{O}_7$ is different from that in bulk $\text{Sr}_3\text{Ru}_2\text{O}_7$. On the basis of the available information, therefore, so far we cannot conclude that $\text{Sr}_3\text{Ru}_2\text{O}_7$ itself is superconducting.

V. SUMMARY

We have studied superconductivity in the $\text{Sr}_3\text{Ru}_2\text{O}_7$ – Sr_2RuO_4 eutectic system. Our AC susceptibility measurements revealed that multiple superconducting transitions occur in the $\text{Sr}_3\text{Ru}_2\text{O}_7$ – Sr_2RuO_4 eutectic sample, and that the transitions with T_c lower than that of Sr_2RuO_4 originate from the $\text{Sr}_3\text{Ru}_2\text{O}_7$ region alone. These experimental results indicate that the superconductivity observed in the $\text{Sr}_3\text{Ru}_2\text{O}_7$ region is not attributable to an unusually-long-range proximity effect across the boundary between Sr_2RuO_4 and $\text{Sr}_3\text{Ru}_2\text{O}_7$. Both T^* and $\Delta\chi'$ of this superconductivity are sensibly suppressed by weak AC magnetic fields. Moreover, their H – T phase diagrams are qualitatively different from that of bulk Sr_2RuO_4 , and no anomaly was observed in the specific heat of the $\text{Sr}_3\text{Ru}_2\text{O}_7$ region sample cut from the eutectic crystals. Although we have not achieved a conclusive explanation of the origin of superconductivity in the $\text{Sr}_3\text{Ru}_2\text{O}_7$ region, we proposed scenarios to explain our experiments. Among them,

the scenario in which Sr_2RuO_4 thin slabs are embedded in the $\text{Sr}_3\text{Ru}_2\text{O}_7$ region and the multiple superconducting transition temperatures arise from the distribution of the slab thickness yielded the most satisfying fit to the experiments.

Acknowledgments

We thank Francesco Tafuri, Manfred Sigrist, Mario Cuoco, Canio Noce, Yukio Tanaka, Yasuhiro Asano, Robin S. Perry, and Andrew P. Mackenzie for valuable discussions, and Kentaro Kitagawa, Hiroshi Takatsu, and Markus Kriener for their support. This work has been supported by Grants-in-Aid for Scientific Research from the Japan Society for Promotion of Science (JSPS) and from the Ministry of Education, Culture, Sports, Science, and Technology of Japan (MEXT). It is also supported by a Grant-in-Aid for the 21st Century COE program “Center for Diversity and Universality in Physics” from MEXT.

-
- ¹ Y. Maeno, H. Hashimoto, K. Yoshida, S. Nishizaki, T. Fujita, J. G. Bednorz, and F. Lichtenberg, *Nature (London)* **372**, 532 (1994).
 - ² A. P. Mackenzie and Y. Maeno, *Rev. Mod. Phys.* **75**, 657 (2003).
 - ³ K. Ishida, H. Mukuda, Y. Kitaoka, K. Asayama, Z. Q. Mao, Y. Mori, and Y. Maeno, *Nature (London)* **396**, 658 (1998).
 - ⁴ G. M. Luke, Y. Fudamoto, K. M. Kojima, M. I. Larkin, J. Merrin, B. Nachumi, Y. J. Uemura, Y. Maeno, Z. Q. Mao, Y. Mori, H. Nakamura, and M. Sgrist, *Nature (London)* **394**, 558 (1998).
 - ⁵ J. Xia, Y. Maeno, P. T. Beyersdorf, M. M. Fejer, and A. Kapitulnik, *Phys. Rev. Lett.* **97**, 167002 (2006).
 - ⁶ Y. Maeno, T. Ando, Y. Mori, E. Ohmichi, S. Ikeda, S. Nishizaki, and S. Nakatsuji, *Phys. Rev. Lett.* **81**, 3765 (1998).
 - ⁷ R. Fittipaldi, A. Vecchione, S. Fusanobori, K. Takizawa, H. Yaguchi, J. Hooper, R. S. Perry, and Y. Maeno, *J. Cryst. Growth* **282**, 152 (2005).
 - ⁸ H. Yaguchi, M. Wada, T. Akima, Y. Maeno, and T. Ishiguro, *Phys. Rev. B* **67**, 214519 (2003).
 - ⁹ H. Yaguchi, K. Takizawa, M. Kawamura, N. Kikugawa, Y. Maeno, T. Meno, T. Akazaki, K. Semba, and H. Takayanagi, *J. Phys. Soc. Jpn* **75**, 125001 (2006).
 - ¹⁰ M. Kawamura, H. Yaguchi, N. Kikugawa, Y. Maeno, and H. Takayanagi, *J. Phys. Soc. Jpn* **74**, 531 (2005).
 - ¹¹ R. S. Perry, K. Kitagawa, S. A. Grigera, R. A. Borzi, A. P. Mackenzie, K. Ishida, and Y. Maeno, *Phys. Rev. Lett.* **92**, 166602 (2004).
 - ¹² R. A. Borzi, S. A. Grigera, R. S. Perry, N. Kikugawa, K. Kitagawa, Y. Maeno, and A. P. Mackenzie, *Phys. Rev. Lett.* **92**, 216403 (2004).
 - ¹³ J. Hooper, M. Zhou, Z. Q. Mao, Y. Liu, R. Perry, and Y. Maeno, *Phys. Rev. B* **73**, 132510 (2006).
 - ¹⁴ K. Deguchi, Z. Mao, and Y. Maeno, *J. Phys. Soc. Jpn* **73**, 1313 (2004).
 - ¹⁵ Z. Q. Mao, Y. Mori, and Y. Maeno, *Phys. Rev. B* **60**, 610 (1999).
 - ¹⁶ K. Deguchi, M. A. Tanatar, Z. Mao, T. Ishiguro, and Y. Maeno, *J. Phys. Soc. Jpn* **71**, 2839 (2002).
 - ¹⁷ Y. Maeno, K. Yoshida, H. Hashimoto, S. Nishizaki, S.-I. Ikeda, M. Nohara, T. Fujita, A. P. Mackenzie, N. E. Hussey, J. G. Bednorz, F. Lichtenberg, *J. Phys. Soc. Jpn* **66**, 1405 (1997).
 - ¹⁸ S.-I. Ikeda, Y. Maeno, S. Nakatsuji, M. Kosaka, and Y. Uwatoko, *Phys. Rev. B* **62**, R6089 (2000).
 - ¹⁹ M. Yang, Y. H. Kao, Y. Xin, and K. W. Wong, *Phys. Rev. B* **50**, 13653 (1994).
 - ²⁰ K. H. Müller, *Physica C* **159**, 717 (1989).
 - ²¹ J. R. Clem, *Physica C* **153-155**, 50 (1988).
 - ²² K. H. Müller, J. C. Macfarlane, and R. Driver, *Physica C* **158**, 69 (1989).
 - ²³ A. Raboutou, J. Rosenblatt, and P. Peyral, *Phys. Rev. Lett.* **45**, 1035 (1980).
 - ²⁴ M. Tinkham, *Introduction to superconductivity*, 2nd ed. (McGraw-Hill, New York, 1996).
 - ²⁵ M. Varela, W. Grogger, D. Arias, Z. Sefrioui, C. León, L. Vazquez, C. Ballesteros, K. M. Krishnan, and J. Santamaria, *Phys. Rev. B* **66**, 174514 (2002).
 - ²⁶ H. Taniguchi, Y. Nakazawa, and K. Kanoda, *Phys. Rev. B* **57**, 3623 (1998).
 - ²⁷ K. Deguchi *et al.*, unpublished.
 - ²⁸ R. Fittipaldi *et al.*, in preparation.
 - ²⁹ H. Shaked, J. D. Jorgensen, S. Short, O. Chmaissem, S. I. Ikeda, and Y. Maeno, *Phys. Rev. B* **62**, 8725 (2000).
 - ³⁰ Q. Huang, J. W. Lynn, R. W. Erwin, J. Jarupatrakorn, and R. J. Cava, *Phys. Rev. B* **58**, 8515 (1998).
 - ³¹ Y. Inoue, M. Hara, Y. Koyama, S. Ikeda, Y. Maeno, and T. Fujita, in *Advances in Superconductivity IX*, edited by S. Nakajima and M. Murakami (Springer-Verlag, Berlin, 1997), p. 281.
 - ³² R. Matzdorf, Z. Fang, Ismail, J. Zhang, T. Kimura, Y. Tokura, K. Terakura, and E. W. Plummer, *Science* **289**, 746 (2000).
 - ³³ O. Friedt, M. Braden, G. Andre, P. Adelman, S. Nakatsuji, and Y. Maeno, *Phys. Rev. B* **63**, 174432 (2001).
 - ³⁴ Z. Fang and K. Terakura, *Phys. Rev. B* **64**, 020509(R) (2001).
 - ³⁵ M. Kriener, P. Steffens, J. Baier, O. Schumann, T. Zabel, T. Lorenz, O. Friedt, R. Müller, A. Gukasov, P. G. Radaelli, P. Reutler, A. Revcolevschi, S. Nakatsuji, Y. Maeno, and M. Braden, *Phys. Rev. Lett.* **95**, 267403 (2005).